# A performance model for the open fan propulsor

Nicolas Tantot[1], Panagiotis Giannakakis[2]*, Henri Yesilcimen[3], Anthony Binder[4]
* Corresponding author
[1] Safran Aircraft Engines, 77550 Moissy-Cramayel, France, nicolas.tantot@safrangroup.com
[2] Safran SA, 78772 Magny-Les-Hameaux, panagiotis.giannakakis@safrangroup.com
[3] Safran Aircraft Engines, 77550 Moissy-Cramayel, France, henri.yesilcimen@safrangroup.com
[4] Safran Aircraft Engines, 77550 Moissy-Cramayel, France, anthony.binder@safrangroup.com

## Abstract

The open fan engine, featuring ultra-high propulsive efficiency, is considered one of the most realistic and sustainable option for civil aviation. The preliminary design of such architectures requires a robust and flexible modeling of the propulsor performance. An innovative approach based on induced velocity models combined with aerodynamic polars is proposed for an open fan consisting of a variable pitch propeller rotor and a variable pitch stator. An assessment of the method accuracy is provided, covering propeller map generation, static and reverse performance, and design parametric studies on diameter, aspect ratio and blades count. The proposed method is a good compromise between accuracy and numerical robustness, usable in a cycle performance model, for both design and off-design studies.

## Nomenclature

| | | | | |
|---|---|---|---|---|
| A | Area, m$^2$ | | Z | Axial distance, m |
| AR | Blade aspect ratio | | α | Sound velocity, m/s |
| c | Chord length, m | | β | Pitch angle, ° |
| $C_L$, $C_D$ | Lift and drag coefficients | | Γ | Circulation, m$^2$/s |
| $C_{P,120}$ | $P_{120}/(\rho_0 \cdot N_{120}{}^3 \cdot D_{120}{}^5)$ | | ε | Calibration exponent |
| D | Tip diameter, m | | η | Efficiency |
| F | Force, N | | λ | Stator clipping |
| $F_N$ | Net thrust, N | | ν | Hub-to-tip ratio |
| i | Angle of attack, rad | | ρ | Air density, kg/m$^3$ |
| k | Calibration coefficient | | φ | Flow angle, rad |
| M | Mach number | | | |
| $N_B$ | Number of blades | | **Subscripts** | |
| $N_{120}$ | Rotor rotational speed, rps | | | |
| Q | Torque, N.m | | 0 | Free-stream |
| $P_{120}$ | Rotor power, W | | d | Drag |
| p | Static pressure, Pa | | h | Hub |
| r | Radius relative to tip | | id | Ideal |
| R | Tip radius, m | | nac | Related to nacelle |
| u | Induced velocity, m/s | | ref | Reference relative radius |
| $U_t$ | Rotor tip speed, m/s | | str | Related to rotor stream-tube |
| V | Velocity, m/s | | z | Axial component |
| w | Wake displacement velocity, m/s | | θ | Tangential component |
| W | Mass flow, kg/s | | | |

## 1. Introduction

A significant breakthrough in propulsive efficiency is expected from next generation unducted aero-engines [1]. These engines, also known as « open-rotor » layouts, feature ultra-low pressure ratio unducted propulsors able to minimize kinetic energy waste. Several options can be imagined for these engines in either pusher or puller configurations:

Nicolas Tantot, Panagiotis Giannakakis, Henri Yesilcimen, Anthony Binder

- Single propeller rotor, known as turboprop configuration.
- Counter-rotating propeller rotors, known as CROR configuration (Counter Rotating Open Rotor).
- Propeller rotor with active variable pitch stator, known as USF (Unducted Single Fan), SRV (Swirl Recovery Vane), ORAS (Open Rotor with Active Stator) or Open Fan.

Although the performance modeling of legacy turboprop is well treated through the use of performance maps covering the rotor behavior at off-design conditions, the modeling of the more complex CROR and USF configurations requires significant adaptations to encompass the additional dimension of the rear propulsor stage behavior. Regarding the CROR configuration, a dedicated method has been proposed to predict the individual and combined off-design behavior of propeller rotors for a given set of blade geometries [2]. The propeller individual rotor map generation process has also been subject to innovative approaches, aiming at making a link between numerical mapping of performance and the aerodynamic behavior of the rotor [3]. Past studies also investigated the possibility of having a common propeller efficiency map for different propeller designs, by separating the induced and viscous losses when creating the propeller map [4], or by scaling an existing propeller map [5].

The design of the USF / Open fan architecture requires extending such modeling approaches, in order to tackle the combination of a variable pitch rotor with a variable pitch stator. A recent work on the USF architecture by Clark et al [6], used blade-element momentum theory to simulate both the rotor and stator, by calculating either extended propeller maps, or "lighter" six point tables, before integrating them with the rest of the engine performance model in the form of a propeller power management schedule. This approach requires the propeller performance to be evaluated individually for every propeller design, before the cycle performance evaluation, which might not be ideal if one wants to concurrently optimize engine and propulsor, while taking into account their interactions.

## 1.1 Work aim and requirements

Considering the specific USF / Open fan engine architecture, a key expectation is to be able to separate the performance of the rotor from the performance of the stator. Indeed, the location of the gas generator inlet after the propeller rotor and before the stator requires the prediction of the thermodynamic conditions after the rotor. In addition, preliminary design activities require the exploration of the propulsor and gas-generator design space and the corresponding impact on the overall engine performance.

Furthermore, performance models are characterized by their ability to be run almost instantaneously, therefore relying on basic 0D or 1D physics. Iterative resolutions should be kept to a minimum number in order to enable such an acceptable behavior. Finally, the performance model should be numerically robust in order to predict any kind of operating condition, from design to extreme off-design ones, with the same convergence rate.

## 1.2 Modeling perimeter

The proposed model is based on the propulsive thrust and efficiency definition [7]. According to this definition, the thrust generated by the open fan takes into account the axial energy rise through the open fan propeller stream-tube. We separate the propeller stream-tube from the core stream-tube based on the mass quantity going into the engine relative to the flow going outside the engine. The calculation starts with the overall propulsive force which is defined as the momentum and pressure force difference on the exit and inlet surfaces of the propeller stream-tube. This force takes into account open fan forces, open OGV forces, nacelle forces and streamline forces (see Figure 1).
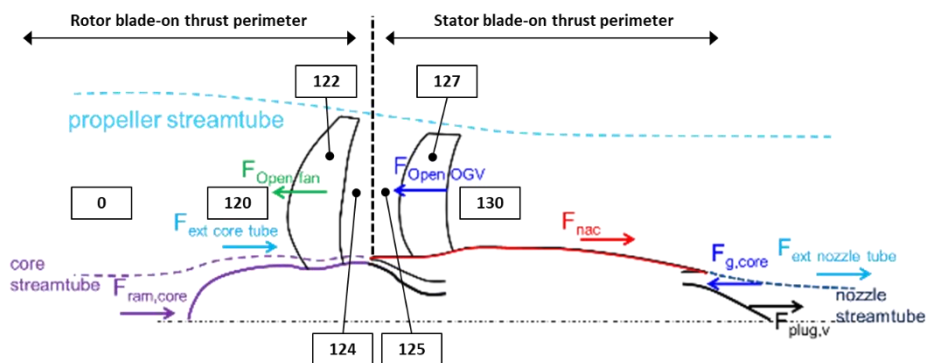


Figure 1 : Forces for the blades-on configuration
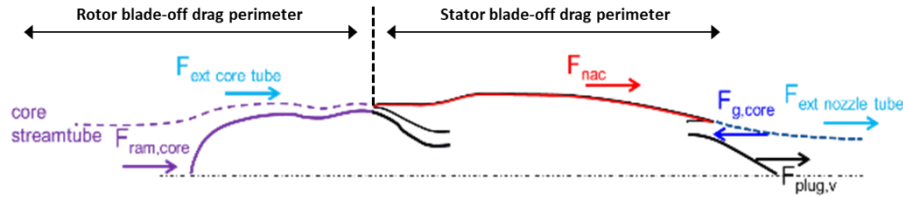
Figure 2 : Forces for the blades-off configuration

To get to the propulsive force, the blade-off forces must be removed from the overall propulsive thrust. The net thrust is then free of the effect of the presence of the nacelle and its drag and gives a better understanding of the actual open fan performance. The idea is to remove the potential flow generated by the nacelle so that we get a more precise estimation of the free-air open fan performance, which is less sensitive to nacelle or spinner design iterations.

$$\mathbf{F_{N,120}} = F_{Open\ fan} + \left( F_{ext\ core\ tube\ Blade-on} - F_{ext\ core\ tube\ Blade-off} \right) \tag{1}$$

$$\mathbf{F_{N,125}} = F_{OGV} + \left( F_{nac\ Blade-on} - F_{nac\ Blade-off} \right) + \left( F_{ext\ nozzle\ tube\ Blade-on} - F_{ext\ nozzle\ tube\ Blade-off} \right) \tag{2}$$

The propulsive efficiency is then computed using this (blades-on – blades-off) net thrust, divided by the power consumption of the open fan in the propeller stream. This means that the blade is theoretically truncated by the stream line between propeller stream and core stream and only the torque above this line is computed.

Therefore, two kinds of calculations are required to get the data for the calibration of the models presented in this paper: blades-on and blades-off. Blades-on calculations include both the open fan and OGV. The calculations should cover several rotational speeds, flight Mach numbers, rotor/OGV pitch angles and core inlet/nozzle flow conditions.

## 2. Rotor modeling

All labels used in this section refer to the Figure 3 below.
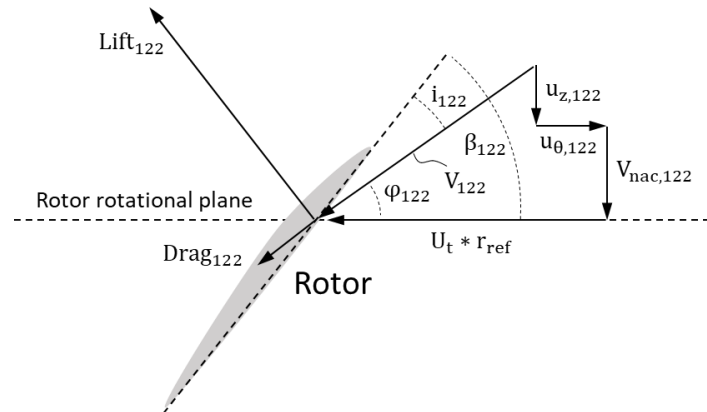


Figure 3 : Rotor velocities and forces

### 2.1 Free-stream velocities, boundary conditions and geometry

The rotor boundary conditions, that should be known before the calculation begins, include: the flight velocity $V_0$, the air density $\rho_0$ and velocity of sound for the given flight condition $\alpha_0$, the rotor tip velocity $U_t$, the rotor pitch angle $\beta_{120}$ and the gas-generator inlet mass flow $W_{20}$. Naturally, the rotor number of blades $N_{B,120}$, hub-to-tip ratio $\nu_{120}$, diameter $D_{120}$ and the rotor aspect ratio $AR_{120}$ should also be known. The relative velocity at the rotor relative reference radius $r_{ref}$ can then be calculated as follows:

$$\mathbf{V_{110}} = \sqrt{V_0{}^2 + (U_t \cdot r_{ref})^2} \tag{3}$$

Nicolas Tantot, Panagiotis Giannakakis, Henri Yesilcimen, Anthony Binder

The rotor relative reference radius $r_{ref}$ is commonly taken equal to 75%, as this is the approximate location of the rotor maximum loading, and the radius at which the rotor pitch angle is defined.

## 2.2 Free-stream velocity including the nacelle effect

The free-stream velocity including the impact of the engine nacelle on the rotor exit plane can be modeled as a function of the flight Mach number and a coefficient calibrated for a representative geometry, as follows:

$$V_{nac,124} = V_0 \cdot \left(1 - k_{nac} \cdot M_0^4\right) \tag{4}$$

The coefficient $k_{nac}$ should be calibrated in order to match the axial velocity at rotor exit estimated by CFD calculations for a cruise condition. The rotor and stator aerodynamic plane velocities (planes 122 and 127 respectively), as well as the stator inlet plane (125) velocities, are obtained by assuming half the rotor exit plane induced velocity effect, i.e. $V_{nac,122} = V_{nac,125} = V_{nac,127} = V_0 \cdot \left(1 - (1 - V_{nac,124}/V_0)/2\right)$.

## 2.3 Rotor plane velocities

The assessment of velocity field in the rotor wake is based on reference [8], simplified in order to calculate the different quantities only for the reference radius $r_{ref}$. It must be underlined that the velocities induced by the stator on the rotor were neglected. The calculation requires iterating on the wake axial displacement velocity[1] w.

According to reference [8], in the rotor wake, the fluid particles are convected by the normal component of the helical wake sheets displacement w (one can picture a solid helical wake "sweeping" the fluid particles). One can then calculate the fluid particles axial and tangential velocities using trigonometric relations, and assuming that at the rotor plane the induced velocities are half of their far downstream values. As full wake contraction is obtained approximately on the stator plane, the free-stream velocity is taken equal to $V_{nac,125}$.

$$u_{z,122,id} = 0.5 \cdot w \cdot \left[1 + \left(V_{nac,122} + w\right)^2 \cdot \left(U_t \cdot r_{ref}\right)^{-2}\right]^{-1} \tag{5}$$

$$u_{\theta,122,id} = 0.5 \cdot w \cdot \left(V_{nac,122} + w\right) \cdot \left(U_t \cdot r_{ref}\right)^{-1} \cdot \left[1 + \left(V_{nac,122} + w\right)^2 \cdot \left(U_t \cdot r_{ref}\right)^{-2}\right]^{-1} \tag{6}$$

Knowing the axial and tangential induced velocities one can then calculate the rotor relative velocity and the corresponding flow angle, and angle of attack.

$$V_{122} = \sqrt{\left(V_{nac,122} + u_{z,122,id}\right)^2 + \left(U_t \cdot r_{ref} - u_{\theta,122,id}\right)^2} \tag{7}$$

$$\varphi_{122} = \tan^{-1}\left(\left(V_{nac,122} + u_{z,122,id}\right)/\left(U_t \cdot r_{ref} - u_{\theta,122,id}\right)\right) \text{ [rad]} \tag{8}$$

$$i_{122} = \frac{\pi}{180} \cdot \beta_{120} - \varphi_{122} \text{ [rad]} \tag{9}$$

The lift coefficient can then be calculated using Prandtl's approximation of the Goldstein function, as follows:

$$f = 2\pi^{-1} \cdot \cos^{-1} \exp\left[-0.5 \cdot {N_{B,120}}\big/{k_{NB,120}} \cdot (1 - r_{ref}) \cdot \sqrt{1 + \left(V_{nac,122} + w\right)^2 \cdot U_t^{-2}} \cdot \left|V_{nac,122} + w\right|^{-1} \cdot U_t\right] \tag{10}$$

$$G = f \cdot r_{ref}^2 \left[r_{ref}^2 + \left(V_{nac,122} + w\right)^2 \cdot U_t^{-2}\right]^{-1} \tag{11}$$

$$C_{L,120} = \begin{cases} 2\pi D_{120}\left(k_{Cp,120} \cdot k_{NB,120}\right)\left(c_{120}N_{B,120}\right)^{-1} \cdot G \cdot w \cdot \max\left(w_m V_{nac,122}, \left|V_{nac,122} + w\right|\right) \cdot \left(V_{122}U_t\right)^{-1} \\ f(i_{122}) \end{cases} \tag{12}$$

---

[1] The velocity with which the helical wake is moving downstream, similar to a solid screw.

In the above equations, the saturation minimum value of $w_m$, and the absolute values were added by the authors in order to cover extreme operating conditions, such as the reverse thrust one. The saturation value $w_m$ is calculated on a reverse thrust, low-speed condition and a typical value would be 0.85. The coefficients $k_{NB,120}$ and $k_{Cp,120}$ are design effect calibrations for the rotor blades number and the rotor load respectively. As explained later in §4.5, these coefficients are equal to one for the reference design for which the lift/drag polars are identified.

The rotor circulation is then calculated in the following manner:

$$\Gamma_{120} = 0.5 \cdot V_{122} \cdot c_{120} \cdot C_{L,120} \tag{13}$$

The iterative scheme on $w$ is closed by equating expression 12 with the lift coefficient calculated using data for appropriate airfoils as function of the rotor angle of attack. In this work, the airfoil aerodynamic performance has been described using analytic expressions, as presented later on.

## 2.4 Rotor exit plane average velocities

The vortex theory, based on the ideal wake assumption, allows to calculate the rotor thrust and torque with sufficient accuracy, but is less accurate when it comes to the actual rotor exit velocities prediction at take-off conditions, where the wake geometry is far from ideal. Furthermore, the induced velocities have been calculated for a reference relative radius of 75% and do not necessarily represent the average values required for defining the flow-field attacking the stator. Hence, one needs to add empirical corrections on top of the ideal values calculated by equations 5 and 6.

First, a corrected rotor aerodynamic plane average axial velocity (station 122) can be calculated as the sum of the nacelle velocity and a modified axial induced velocity, using the correction given below as function of the flight speed and of the wake contraction (expressed by the ratio of velocities of Eq. 14). This velocity will be used later on for a more accurate calculation of the rotor mass flow.

$$\mu = \left(V_0 + 2 \cdot u_{z,122,id}\right) \cdot \left(V_0 + u_{z,122,id}\right)^{-1} \tag{14}$$

$$k_{z,122} = \begin{cases} \min\left(2^{\varepsilon_z}, k_{z,122,max}\right) & V_0 \leq 0 \\ 1 & V_0 > 0 \;\&\; u_{z,122,id} \leq 0 \\ \min\left(\mu^{\varepsilon_z}, k_{z,122,max}\right) & V_0 > 0 \;\&\; u_{z,122,id} > 0 \end{cases} \tag{15}$$

$$V_{z,122} = V_{nac,122} + k_{z,122} \cdot u_{z,122,id} \tag{16}$$

Taking the rotor inlet as the axial distance reference ($Z_{120} = 0$), one can assume that the rotor exit axial distance is equal to the average rotor chord ($Z_{124} = c_{120}$). The rotor exit axial velocity is calculated as the sum of the nacelle velocity $V_{nac,124}$, and the "average" induced velocity $\left(k_{z,122} \cdot u_{z,122,id}\right)$ corrected for the flow stream contraction for the axial position $z_{124}$, as shown in Eq. 17.

$$V_{z,124} = V_{nac,124} + k_{z,122} \cdot u_{z,122,id} \cdot \left[1 + Z_{124} \cdot \left(Z_{124}{}^2 + R_{120}{}^2\right)^{-0.5}\right] \tag{17}$$

The parameters $\varepsilon_z$ and $k_{z,122,max}$ need to be calibrated using CFD calculations for a representative geometry. More specifically, $\varepsilon_z$ is calculated on a take-off condition by matching the mass-average axial velocity calculated using CFD at rotor exit, with the ideal one estimated by Eq. 17. The saturation parameter $k_{z,122,max}$ is calculated in the same manner based on an average axial velocity representative of static conditions.

Turning now to the tangential velocities, the stator model requires the precise calculation of its mass average on the rotor exit plane, used for the stator global performance calculations, and of its localized value on the reference radius where the stator pitch is defined, i.e. at 75% of the stator tip radius. Knowing that at rotor exit the tangential velocity is twice the one in the rotor aerodynamic plane, and that the wake-induced velocities have already been calculated for the reference radius of 75%, one can estimate the rotor exit tangential velocity at 75% of the tip radius as follows:

$$V_{\theta,124,@r_{ref}} = 2 \cdot u_{\theta,122,id} \cdot k_{NB,120} \cdot k_{Cp,120}{}^{-1} \tag{18}$$

Subsequently, one can correct the local velocity, in order to obtain the mass-averaged one, as follows:

Nicolas Tantot, Panagiotis Giannakakis, Henri Yesilcimen, Anthony Binder

$$V_{\theta,124} = V_{\theta,124,@r_{ref}} \cdot (r_{ref}/\bar{r}_\theta) \tag{19}$$

The radius $\bar{r}_\theta$, corresponding to the average tangential velocity, is given as a function of the rotor circulation:

$$\bar{r}_\theta = (\bar{r}_{\theta,max} - \bar{r}_{\theta,min}) \cdot \left[1 - \exp\left(-\bar{r}_{\theta,a} \cdot |\Gamma_{120}/\Gamma_{120,des}|\right)\right]^8 + \bar{r}_{\theta,min} \tag{20}$$

The parameter $\Gamma_{120,des}$ is the rotor circulation on the cruise design point. Table 1 gives typical values for the different parameters of Eq. 18, as a function of the relative Mach number based on $V_{110}$, determined by comparing the mass-averaged rotor exit tangential velocity calculated by CFD with the one given by the model. The CFD calculations should cover several flight conditions and pitch angles.

| $M_{110}$ | $< 0.750$ | $= 0.825$ | $> 0.900$ |
|---|---|---|---|
| $\bar{r}_{\theta,max}$ | 0.715 | 0.700 | 0.685 |
| $\bar{r}_{\theta,min}$ | 0.650 | 0.575 | 0.250 |
| $\bar{r}_{\theta,a}$ | 2.735 | 3.830 | 4.375 |
| Interpolation | | Linear | |

Table 1 : Typical values of the calibration coefficients for the rotor exit tangential velocity

It should be underlined that the calculation of all calibration coefficients is conducted by imposing for each operating condition the rotor thrust and torque calculated by CFD, while the lift and drag coefficient are free to vary. In that manner the flow field will be calibrated for the target rotor performance.

## 2.5 Rotor aerodynamic hub radius

As explained in §1.2, the propulsor thrust does not include the flow-stream ingested by the engine gas generator. Hence, the integration of blade forces should be carried out starting from the "aerodynamic" hub radius, defined by the stream-line separating what is ingested by the engine core, from the rest of the propulsor mass flow. The rotor mass flow can be calculated using the rotor total area and the previously estimated axial velocity for the rotor aerodynamic plane, Eq. 21. A lower limit is added equal to the ingested mass flow, to cater for extreme operating cases where the propeller does not produce the necessary flow.

$$W_{120} = \max\left(W_{20}, \ \rho_0 \cdot |V_{z,122}| \cdot \pi \cdot R_{120}{}^2 \cdot (1 - \nu_{120}{}^2)\right) \tag{21}$$

The aerodynamic hub radius can then be calculated as follows:

$$R_{h,120,aero} = R_{120} \cdot \min\left([1 - (W_{120} - W_{20})/W_{120} \cdot (1 - \nu_{120}{}^2)]^{0.5}, \ 1.5 \cdot \nu_{120}\right) \tag{22}$$

## 2.6 Rotor global performance

By integrating along the rotor blades height starting from the aerodynamic hub radius, one can calculate the total rotor thrust, torque and efficiency, using the following equations:

$$F_{N,120} = \frac{\rho_0}{2} \cdot N_{B,120} \cdot c_{120} \cdot V_{122}{}^2 \cdot (C_{L,120} \cdot \cos \varphi_{122} - C_{D,120} \cdot \sin \varphi_{122}) \cdot (R_{120} - R_{h,120,aero}) \tag{23}$$

$$Q_{120} = \frac{\rho_0}{2} \cdot N_{B,120} \cdot c_{120} \cdot V_{122}{}^2 \cdot (C_{L,120}\sin\varphi_{122} + C_{D,120}\cos\varphi_{122})(R_{120} - R_{h,120,aero}) \cdot r_{ref} \cdot R_{120} \tag{24}$$

The rotor chord $c_{120}$ can be calculated from the rotor height and aspect ratio. Rotor efficiency is then:

$$\eta_{120} = (F_{N,120} \cdot V_0)/(Q_{120} \cdot U_t \cdot R_{120}{}^{-1}) \tag{25}$$

## 2.7 Rotor lift and drag polars

Similar to the calculation of the flow-field calibration coefficients, the calibration of the rotor lift and drag polars is performed by imposing the rotor thrust and torque for a given operating condition. The lift and drag coefficient are therefore a fallout of the calculation.

Starting with the lift coefficient, the CFD calculations carried out for a modern open-fan geometry indicated that lift is an almost linear function of the angle of attack, but with a separate slope for positive and negative angles of attack. Furthermore, the lift coefficient was found to also be a function of $M_{110}$ and on the velocities ratio $(V_0/U_t)$. Taking into account all these considerations, the following equations were implemented:

$$C_{L,120} = \begin{cases} C_{L,0,120} + C_{L,a-,120} \cdot \sin(i_{122} - i_{0,122}) & i_{122} \leq i_{0,122} \\ C_{L,0,120} + C_{L,a+,120} \cdot \sin(i_{122} - i_{0,122}) & i_{122} > i_{0,122} \end{cases} \quad (26)$$

In the above equation, the coefficients $C_{L,0,120}, C_{L,a-,120}, C_{L,a+,120}$ and $i_{0,122}$ are tabulated as functions of $M_{110}$ and the velocities ratio $(V_0/U_t)$ to best fit the lift coefficient calculated by imposing the CFD thrust and torque values.

With respect to the drag coefficient, it is expressed as a function of the lift coefficient, in addition to the previously mentioned dependencies on $M_{110}$ and on the velocities ratio $(V_0/U_t)$.

$$C_{D,120} = \begin{cases} C_{D,ml,120} + C_{D,a1-,120}(C_{L,120} - C_{L,ml,120})^2 + C_{D,a2-,120}(C_{L,120} - C_{L,ml,120})^4 & C_{L,120} \leq C_{L,ml,120} \\ C_{D,ml,120} + C_{D,a1+,120}(C_{L,120} - C_{L,ml,120})^2 + C_{D,a2+,120}(C_{L,120} - C_{L,ml,120})^4 & C_{L,120} > C_{L,ml,120} \end{cases} \quad (27)$$

Similar to the lift equation, the coefficients $C_{D,ml,120}, C_{L,ml,120}, C_{D,a1-,120}, C_{D,a1+,120}$ are tabulated as functions of $M_{110}$ and the velocities ratio $(V_0/U_t)$ to best fit the drag coefficient calculated by imposing the CFD thrust and torque values. On the other hand, $C_{D,a2+,120}$ is calculated for a typical take-off condition and kept constant. $C_{D,a2-,120}$ is calculated for a typical reverse condition and kept constant too.

## 2.8 Adaptation for a standalone propeller rotor

The model presented in the previous paragraphs can also be used to simulate a conventional standalone propeller rotor, with only one minor adaptation. The aerodynamic hub radius can be set equal to the propeller geometric radius, i.e. $R_{h,120,aero} = R_{h,120}$, in which case the engine inlet conditions need to be calculated based on the velocities of §2.4. Furthermore, if one is interested in the propeller rotor global performance and requires only a first order estimation of engine inlet conditions (their impact on global engine performance is generally less than 1%), the model calibration requires the definition of only the rotor polars described in §2.7 (i.e. eight 2D tables and 2 coefficients). Simpler rotor polar formulations could also be envisaged, depending on the level of precision required.

## 3. Stator modeling

All labels used in this section refer to Figure 4. The stator modeling employs a blade element approach applied on a single radius, coupled with a self-induced velocity calculation based on the theory of thin elliptic wings. It should be underlined here that the stator model can be decoupled from the rotor one. As a matter of fact, although the stator performance prediction requires a few input from the upstream rotor model, the way this rotor is modelled can be freely chosen. For example, one can choose to replace the rotor model described in the previous paragraphs, with an interpolation of a conventional propeller map.

## 3.1 Geometry

Apart from the stator pitch angle $\beta_{125}$ that needs to be defined for each operating condition, one should also provide the stator axial distance from the rotor $Z_{125}$, the stator clipping $\lambda_{125}$, the stator hub radius $R_{h,125}$ (it can also be defined relative to the rotor one), the stator number of blades $N_{B,125}$ and the stator aspect ratio $AR_{125}$. The stator diameter can be calculated from the rotor diameter, rotor hub-to-tip ratio and the given clipping in the following manner:

$$D_{125} = D_{120} \cdot [\nu_{120} + \lambda_{125} \cdot (1 - \nu_{120})] \quad (28)$$

Nicolas Tantot, Panagiotis Giannakakis, Henri Yesilcimen, Anthony Binder

The stator chord $c_{125}$ can be calculated from the stator height and aspect ratio.
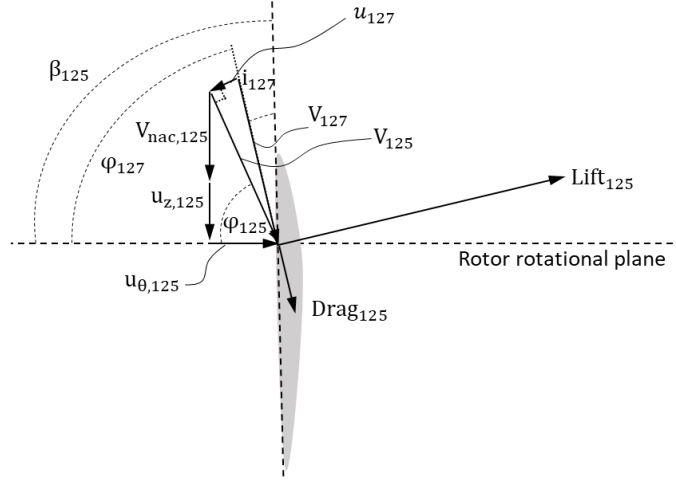


Figure 4 : Stator velocities and forces

## 3.2 Stator inlet plane velocities

Before getting into the stator performance calculation, one needs to transpose the velocities calculated for the rotor exit plane 124, to the stator inlet plane 125. In order to do this, one needs to know the axial distance between the stator and rotor aerodynamic planes and use it in order to calculate the stator axial position $Z_{125}$. The rotor stream-tube axial velocity is then calculated at the stator inlet plane as the sum of the nacelle velocity $V_{nac,125}$, and the "average" rotor induced velocity $\left(k_{z,122} \cdot u_{z,122,id}\right)$ corrected for the flow stream contraction for the axial position $Z_{125}$, as shown in Eq. 29. The equivalent tangential velocity can be taken equal to the average tangential velocity at rotor outlet, i.e. $V_{\theta,str,125} = V_{\theta,124}$.

$$V_{z,str,125} = V_{nac,125} + k_{z,122} \cdot u_{z,122,id} \cdot \left[1 + Z_{125} \cdot \left(Z_{125}^2 + R_{120}^2\right)^{-0.5}\right] \tag{29}$$

After having calculated the velocities in the rotor stream-tube, one needs to differentiate the operating scenarios shown in Figure 5 and described in the following paragraphs, in order to estimate the stator tangential inlet velocities. With respect to the stator axial inlet velocity, this quantity can be estimated by assuming $V_{z,125} = V_{z,str,125}$, without any significant impact on accuracy.

$$\left(V_{z,str,125}/V_{z,122}\right)_{sat} = \begin{cases} 1 + Z_{125} \cdot \left(Z_{125}^2 + R_{120}^2\right)^{-0.5} & V_0 \leq 0 \\ 1 & V_0 > 0 \ \& \ u_{z,122,id} \leq 0 \\ V_{z,str,125}/V_{z,122} & V_0 > 0 \ \& \ u_{z,122,id} > 0 \end{cases} \tag{30}$$

$$R_{t,str,125} = R_{120} \cdot \left[\left(1 - R_{h,120,aero}^2 \cdot R_{120}^{-2}\right) \cdot \left(V_{z,str,125}/V_{z,122}\right)_{sat}^{-1} + R_{h,125}^2 \cdot R_{120}^{-2}\right]^{0.5} \tag{31}$$

$$A_{str,125} = \pi \cdot \left(R_{t,str,125}^2 - R_{h,125}^2\right) \tag{32}$$

$$k_\theta = \max\left(1, k_{\lambda,125} \cdot \left[R_{str,125}/R_{125}\right]^{\varepsilon_\theta}\right) \cdot \min\left(A_{str,125}/A_{125}, 1\right) \tag{33}$$

$$V_{\theta,125} = V_{\theta,str,125} \cdot k_\theta \tag{34}$$

For the operating condition where the stator tip radius is inside the stream-tube (left side of Figure 5), the stator sees only part of the rotor exit flow. Hence, one needs to correct the average tangential velocity attacking the stator. Equation 33 proposes such a correction, where the first term is a function of the stream-tube radius, relative to the stator radius. Equations 30 and 31 are used in order to calculate the required stream-tube radius, from the upstream rotor induced

axial velocity. This correction is saturated to one when the stream-tube radius is lower than the stator one. The calibration exponent $\varepsilon_\theta$ is calculated by matching the averaged stator inlet tangential velocity calculated with CFD for both a take-off and cruise conditions.
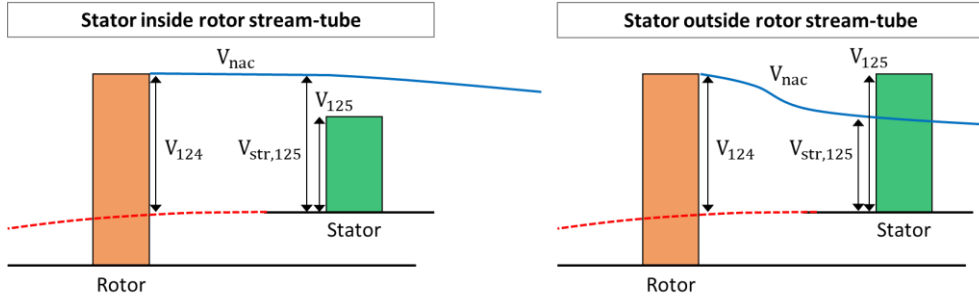


Figure 5 : Operating scenarios for calculating the stator inlet velocities

When, on the other hand, the stator radius is higher than the stream-tube radius, the stator is fed both by the rotor exit flow and by "external flow". Assuming, that the tangential velocity is zero outside the stream-tube, the second term of Eq. 33 corrects for this phenomenon by multiplying the averaged rotor exit velocity with the ratio of the stream-tube area (calculated using Eq. 32), to the stator area. Once more, this correction is saturated to one, for the case where the stream-tube area is higher than the stator area. Consequently, the stator thrust decreases, if its diameter becomes larger than the rotor stream-tube. The calibration coefficient $k_{\lambda,125}$ is used to capture the stator clipping effect (cf. §4.5).

Finally, the total stator inlet velocity and flow angle can be calculated as follows:

$$V_{125} = \sqrt{V_{z,125}^2 + V_{\theta,125}^2} \tag{35}$$

$$\varphi_{125} = \begin{cases} \tan^{-1}(|V_{z,125}|/V_{\theta,125}) & V_{\theta,125} > 0 \\ \tan^{-1}(|V_{z,125}|/V_{\theta,125}) + \pi & V_{\theta,125} \le 0 \end{cases} \quad \text{[rad]} \tag{36}$$

## 3.3 Stator plane velocities

According to the theory describing the flow around finite wings, the wing vortex sheet and especially the tip vortices induce a velocity component, called "downwash" that is perpendicular to the free-stream velocity and opposite in sign to the lift force vector [9]. For the stator case, the free-stream velocity is represented by the one created by the presence of the rotor, as calculated by equations 35 and 36. Similar to the rotor, the calculation requires iterating on the stator induced velocity $u_{127}$ (downwash) divided by the stator upstream velocity $V_{125}$. Knowing the downwash allows the calculation of the induced velocity axial and tangential components:

$$u_{z,127} = u_{127} \cdot \cos \varphi_{125} \tag{37}$$

$$u_{\theta,127} = u_{127} \cdot \sin \varphi_{125} \tag{38}$$

Finally, the total stator plane velocity and flow angle can be calculated as follows:

$$V_{127} = \sqrt{(V_{z,125} + u_{z,127})^2 + (V_{\theta,125} - u_{\theta,127})^2} \tag{39}$$

$$\varphi_{127} = \begin{cases} \tan^{-1}(|V_{z,125} + u_{z,127}|/(V_{\theta,125} - u_{\theta,127})) & V_{\theta,125} - u_{\theta,127} > 0 \\ \tan^{-1}(|V_{z,125} + u_{z,127}|/(V_{\theta,125} - u_{\theta,127})) + \pi & V_{\theta,125} - u_{\theta,127} \le 0 \end{cases} \quad \text{[rad]} \tag{40}$$

As discussed in §2.4, the above velocities represent the average flow-field seen by the stator, and the ones that will be used to calculate its performance. However, as the stator pitch angle is defined for the reference relative radius of 75%, the angle of attack that corresponds to this pitch should also be defined based on a more localized view of the flow-

Nicolas Tantot, Panagiotis Giannakakis, Henri Yesilcimen, Anthony Binder

field, for this specific relative radius. This is achieved in the following equations, which are based on the local, reference radius rotor exit tangential velocity calculated by Eq. 18.

$$V_{\theta,127,@r_{ref}} = k_\theta \cdot V_{\theta,124,@r_{ref}} - u_{\theta,127} \tag{41}$$

$$\varphi_{127,@r_{ref}} = \begin{cases} \tan^{-1}\left(\left|V_{z,125} + u_{z,127}\right|/V_{\theta,127,@r_{ref}}\right) & V_{\theta,127,@r_{ref}} > 0 \\ \tan^{-1}\left(\left|V_{z,125} + u_{z,127}\right|/V_{\theta,127,@r_{ref}}\right) + \pi & V_{\theta,127,@r_{ref}} \le 0 \end{cases} \quad [\text{rad}] \tag{42}$$

$$i_{127} = \frac{\pi}{180} \cdot \beta_{125} - \varphi_{127,@r_{ref}} \; [\text{rad}] \tag{43}$$

The lift coefficient can then be calculated using the Kutta-Joukowski theorem, assuming an elliptical wing planform, high aspect ratio and thin airfoils:

$$C_{L,125} = \begin{cases} \pi \cdot k_{NB,125} \cdot AR_{125} \cdot k_j^{-1} \cdot u_{127} \cdot V_{125}^{-1} \\ f(i_{127}) \end{cases} \tag{44}$$

Given that the stator geometry does not have an elliptical planform, the calibration coefficient $k_j$ has been added. This coefficient is calibrated in order to obtain a matching between the optimal stator aspect ratio obtained with the model, and the one obtained with a higher fidelity method. The calibration coefficient $k_{NB,125}$ improves the modelling of the stator blades count effect (cf. §4.5) and is equal to one for the reference design for which the polar is identified.

Similar to the rotor, the iterative scheme on $u_{127}$ is closed by equating expression 44 with the lift coefficient calculated using data for appropriate airfoils as function of the stator angle of attack. This can be achieved with the analytical expressions that will be presented further on.

## 3.4 Stator global performance

By integrating along the stator blades height starting from the hub radius, one can calculate the total stator thrust, stator torque and propulsor total efficiency, using the following equations:

$$F_{N,125} = \frac{\rho_0}{2} \cdot N_{B,125} \cdot c_{125} \cdot V_{127}^2 \cdot \left(C_{L,125} \cos\varphi_{127} - C_{D,125} \sin\varphi_{127}\right)\left(R_{125} - R_{h,125}\right) + k_p \cdot A_{125} \cdot p_0 \tag{45}$$

$$Q_{125} = \frac{\rho_0}{2} \cdot N_{B,125} \cdot c_{125} \cdot V_{127}^2 \cdot \left(C_{L,125} \sin\varphi_{127} + C_{D,125} \cos\varphi_{127}\right)\left(R_{125} - R_{h,125}\right) \cdot r_{ref} \cdot k_Q \cdot R_{125} \tag{46}$$

$$\eta_{tot} = \left(F_{N,120} + F_{N,125}\right) \cdot V_0 / \left(Q_{120} \cdot U_t \cdot R_{120}^{-1}\right) \tag{47}$$

The coefficient $k_Q$ is calibrated in order to match the averaged swirl angle at the stator exit, calculated with CFD for typical take-off and cruise conditions. It should be noted that the same $r_{ref}$ should be used for the rotor and stator. The stator thrust is complemented with a static pressure term that corresponds to the pressure forces on the surface of the stator blade hub, calibrated for a given geometry using the $k_p$ coefficient (constant between different designs).

## 3.5 Stator lift and drag polars

As for the rotor polars, the calibration of the stator lift and drag polars is performed by imposing the stator thrust and torque for a given operating condition. At the same time, the rotor should operate at the rotational speed and power of the target aerodynamic data.
Starting with the lift coefficient, the CFD calculations carried out for a modern open-fan geometry indicated that lift is an almost linear function of the angle of attack. Furthermore, the lift coefficient was found to also be a function of $M_{110}$ and on the velocities ratio $(V_0/U_t)$. As a result, the following equation was implemented:

$$C_{L,125} = C_{L0,125} + C_{L,a,125} \cdot \sin(i_{127}) \tag{48}$$

In the above equation, the coefficients $C_{L,0,125}$ and $C_{L,a,125}$ are tabulated as functions of $M_{110}$ and the velocities ratio $(V_0/U_t)$ to best fit the lift coefficient calculated by imposing the CFD thrust and torque values. With respect to the drag coefficient, this is expressed as a function of the lift coefficient, in addition to the previously mentioned dependencies on $M_{110}$ and on the velocities ratio $(V_0/U_t)$.

$$C_{D,125} = \begin{cases} C_{D,ml,125} + C_{D,a-,125} \cdot \left[\cosh\left(C_{L,125} - C_{L,ml,125}\right)^{\varepsilon_{d-}} - 1\right] & C_{L,125} \leq C_{L,ml,125} \\ C_{D,ml,125} + C_{D,a+,125} \cdot \left[\cosh\left(C_{L,125} - C_{L,ml,125}\right)^{\varepsilon_{d+}} - 1\right] & C_{L,125} > C_{L,ml,125} \end{cases} \tag{49}$$

Similar to the lift equation, the coefficients $C_{D,ml,125}, C_{L,ml,125}, C_{D,a-,125}, C_{D,a+,125}$ are tabulated as functions of $M_{110}$ and the velocities ratio $(V_0/U_t)$ to best fit the drag coefficient calculated by imposing the CFD thrust and torque values. On the other hand, the exponents $\varepsilon_{d-}$ and $\varepsilon_{d+}$ are calculated to minimize the fitting errors of the drag coefficient for a given lift coefficient on all conditions and kept constant.

## 4. Case study

The following paragraphs present an application of the method on a modern open fan geometry, including a validation with respect to CFD calculations on a few design points, the demonstration of the method's off-design calculations capacity including extreme operation conditions, and finally the verification of the method's design capabilities.

### 4.1 Propulsor specification and geometry

All the results shown in the following sections are based on the top level requirements given in Table 2 below. Unless otherwise stated, the stator pitch angle is set on its optimal value in terms of total efficiency for each operating point.

|  | Take-off | Max-climb | Cruise |
|---|---|---|---|
| Altitude | 0 ft | 35000 ft | 37000 ft |
| Mach | 0.25 | 0.8 | 0.8 |
| $U_t$ | 800 ft/s | 680 ft/s | 680 ft/s |
| $F_N$ | 23000 lbf | 5100 lbf | 4100 lbf |
| $W_{20}$ | 110 lbm/s | 40 lbm/s | 35 lbm/s |
| $\beta_{125}$ | Optimal | Optimal | Optimal |

Table 2 : Propulsor specification points

The objective function for the design studies, is the efficiency averaged on the above three points, with a 5% contribution for take-off, 32% for max-climb and 54% for cruise. The Table 3 below gives the reference geometrical parameters for the rotor and stator.

|  | Rotor | Stator |
|---|---|---|
| Diameter | 13 ft | 12.5 ft |
| Hub to tip ratio | 0.25 | 0.3 |
| Number of blades | 12 | 10 |
| Aspect ratio | 3 | 3 |

Table 3 : Baseline propulsor geometrical parameters

### 4.2 Model validation

For the above geometrical parameters and specification points, a 3D propulsor geometry has been designed, and CFD calculations have been carried out for 150 operating points. The calibration presented here was based on 22 take-off points, 14 max-climb, 14 cruise, 14 approach, 16 flight-idle, 14 reverse thrust and 14 for static conditions. These data have been used in order to calculate the different coefficients and the rotor/stator lift and drag analytical expressions. This included the calibration of a total of 11 constants, three one-dimensional tables and 14 two-dimensional tables (4 additional coefficients are required in order to calibrate the design variations described in §4.5). Subsequently, the model predictions have been compared with the CFD calculations for different flight conditions, by imposing the same rotor speed and power, the same stator pitch angle and the same inlet core flow between the two. The figure below presents the discrepancies between the two for different operating points in terms of rotor thrust and propulsor total

Nicolas Tantot, Panagiotis Giannakakis, Henri Yesilcimen, Anthony Binder

thrust. It is readily seen that the model predictions are close to the CFD results. Although not shown here, rotor pitch discrepancies are lower than 0.10°.
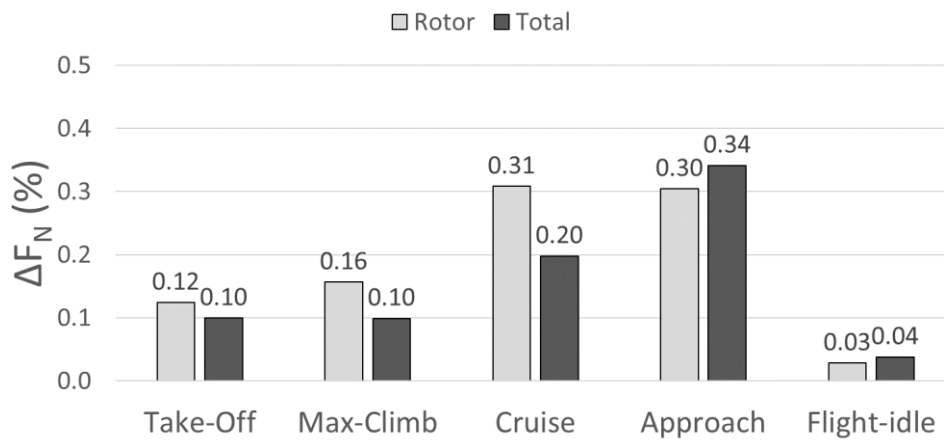


Figure 6 : Validation of the model against CFD results

## 4.3 Map generation

With a calibrated and validated model, it is fairly fast and robust to generate an entire propeller for a given relative Mach number $M_{110}$, many different rotor pitch angles and the stator pitch angle that is optimized for each operating point to attain the best overall propulsor efficiency. The generated map representing the global propulsor performance in Figure 7 for $M_{110} = 0.93$ (typical max-cruise condition). It should be underlined that the relative Mach number is preferred to the flight Mach number, as the map topology does not change significantly between different relative Mach numbers. By observing the different operating points on the maps, one can see that the cruise and climb points are close to the total performance optimum location, which confirms that the propeller optimization achieved its target. Finally, one can notice a visible kink point on the constant rotor pitch lines, which is related to the two-branch modeling of the rotor lift coefficient (Eq. 26).
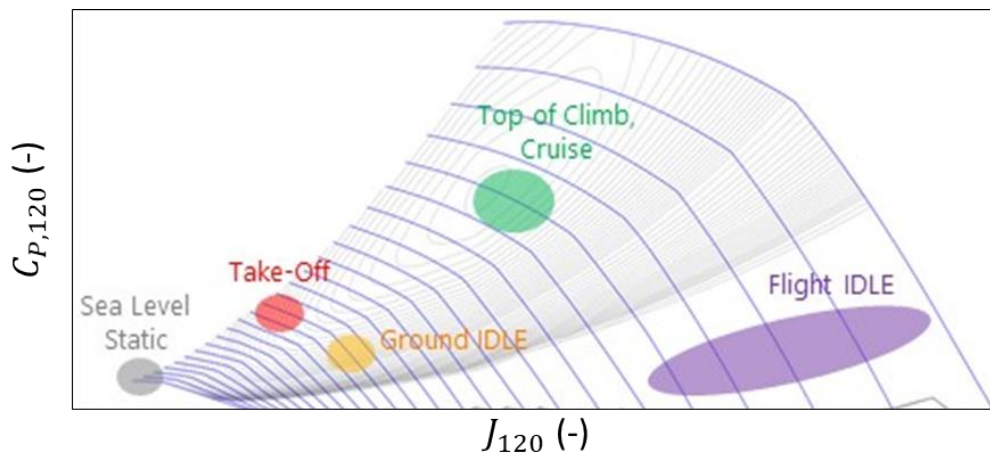


Figure 7 : Rotor and stator combined performance

## 4.4 Extreme operating conditions

The proposed modeling approach is also capable of predicting more extreme operating points, notably the static and reverse conditions. Figure 8 compares the model predictions for a sea-level static condition, for a given rotor speed, and given stator pitch angle. It is shown that the model is very close to the CFD calculations up to the power level where stall begins, and the model starts over-estimating the generated thrust.
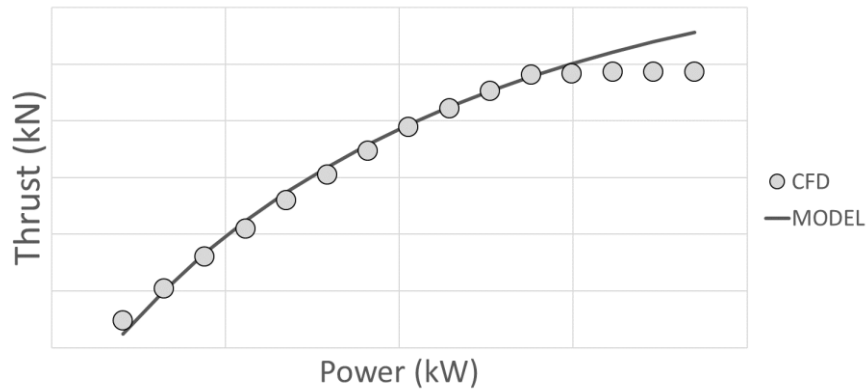
Figure 8 : Static condition prediction compared to CFD results

Figure 9 compares the models predictions with CFD simulations for a sea-level, $M_0 = 0.15$ condition. As shown, the model achieves similar results with the CFD calculation. More specifically, the model accurately predicts the pitch angle that gives the minimum power, which is an important parameter for the control system design. Furthermore, the model accurately estimates the propulsor drag for a typical aircraft landing operating point, which is an important information for the aircraft manufacturer.
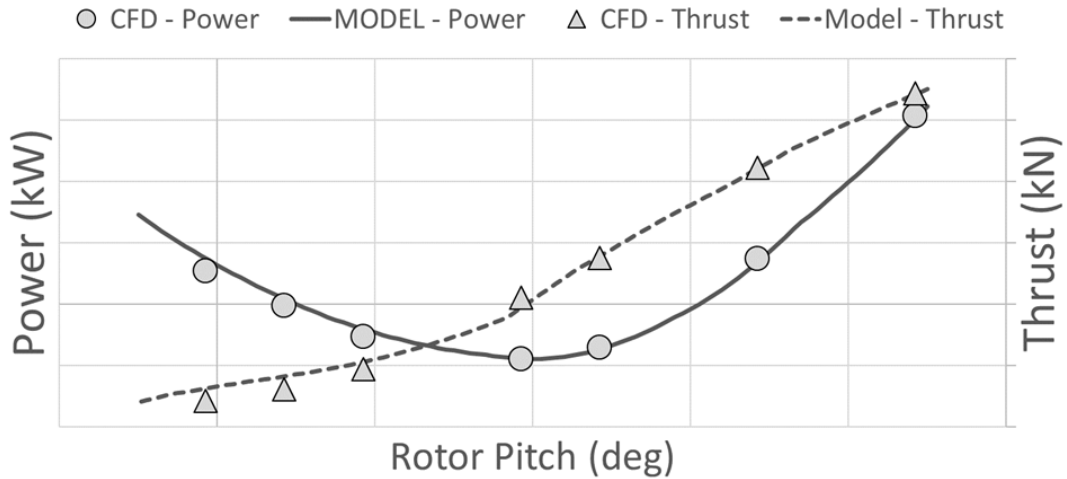


Figure 9 : Reverse condition prediction compared to CFD results

## 4.5 Design studies

A significant advantage of the approach proposed in this paper is the capability to carry out design studies around a given geometry, both for the rotor and stator modules. In order to do that, it is necessary to identify the four calibration exponents $\varepsilon_{Cp,120}$, $\varepsilon_{\lambda,125}$, $\varepsilon_{NB,120}$, $\varepsilon_{NB,125}$ defined by equations 50-53. These calibration exponents are calculated using target efficiency variations calculated for a few geometry modifications, starting from the reference design geometry for which the lift and drag polars have been identified. They can then be kept constant.

$$k_{Cp,120} = \left( C_{P,120} \middle/ C_{P,120 \, @Design \, Ref} \, @Cruise \, Design \, Point \right)^{\varepsilon_{Cp,120}} \tag{50}$$

$$k_{\lambda,125} = \left( \lambda_{125} \middle/ \lambda_{125 \, @Design \, Ref} \right)^{\varepsilon_{\lambda,125}} \tag{51}$$

$$k_{NB,120} = \left( N_{B,120} \middle/ N_{B,120 \, @Design \, Ref} \right)^{\varepsilon_{NB,120}} \tag{52}$$

Nicolas Tantot, Panagiotis Giannakakis, Henri Yesilcimen, Anthony Binder

$$k_{NB,125} = \left( N_{B,125} \Big/ N_{B,125 \, @Design \, Ref} \right)^{\varepsilon_{NB,125}} \tag{53}$$

Turning now to the design case studies, the rotor and stator aspect ratio is proportional to the blade chord for a fixed diameter and controls the value of the lift coefficient. As shown in Figure 10, the choice of aspect ratio considered in the sample geometry used leads to a rotor lift coefficient slightly to the left of the optimum for the cruise condition and slightly to the right of the optimum for the climb (although not shown here, the same is true for the stator).

Figure 11 illustrates that this gives an optimum choice of aspect ratio in terms of weighted efficiency, both for the rotor and stator, which confirms that the coefficient $k_j$ has been calibrated correctly against the CFD simulations. The model is capable of predicting the aspect ratio impact by correctly capturing the effect on the position on the drag polars, and the impact on the induced velocities.
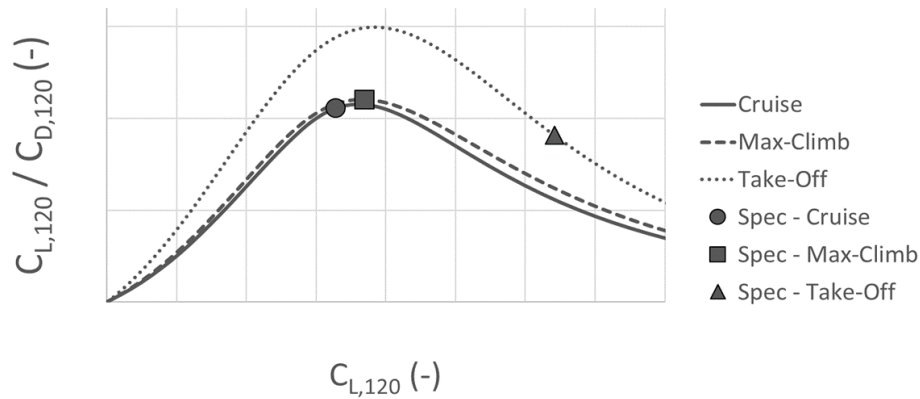


Figure 10 : Aspect ratio optimization effect on rotor lift coefficient and aerodynamic efficiency
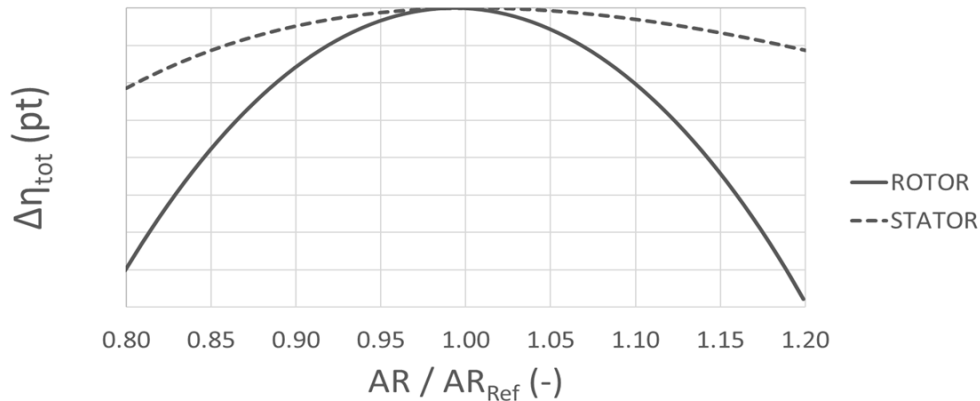


Figure 11 : Aspect ratio optimization in terms of weighted efficiency for the rotor and stator

Figure 12 presents the model prediction when the rotor diameter changes. For this study, the rotor and stator aspect ratios have been optimized for each diameter value, while all other geometric parameters are kept constant (hub-to-tip ratio, blades number and stator clipping). The results show that the model accurately matches the CFD results, with higher efficiencies predicted for higher diameter values.

Figure 13 presents the model prediction when the stator diameter changes for a fixed rotor diameter, i.e. the clipping effect. The modified stator diameter was achieved using a constant stator hub radius and a constant stator mean chord, leading to variations of stator hub-to-tip ratio and aspect ratio. For a clipping variation of up to 10%, the model is in agreement with the only CFD calculation available. Furthermore, the model correctly predicts a degradation in performance when the stator tip radius becomes larger than the rotor stream-flow.

Figure 14 presents the model prediction when the number of blades changes for the rotor and stator, from the reference values of 14/12 to a reduced count of 12/10. For this study, the diameter and hub-to-tip ratio has been kept constant

for both stages, while their aspect ratio varied to maintain the same solidity. The results show that the model gives satisfactory predictions relative to the CFD simulation, with decreased performance for the lower blade count.
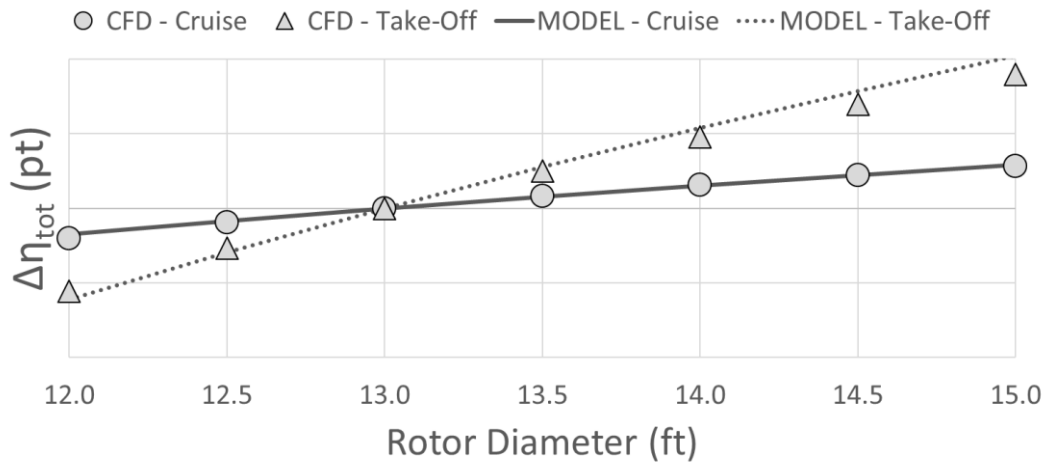
Figure 12 : Rotor diameter effect predicted with the model, compared with CFD
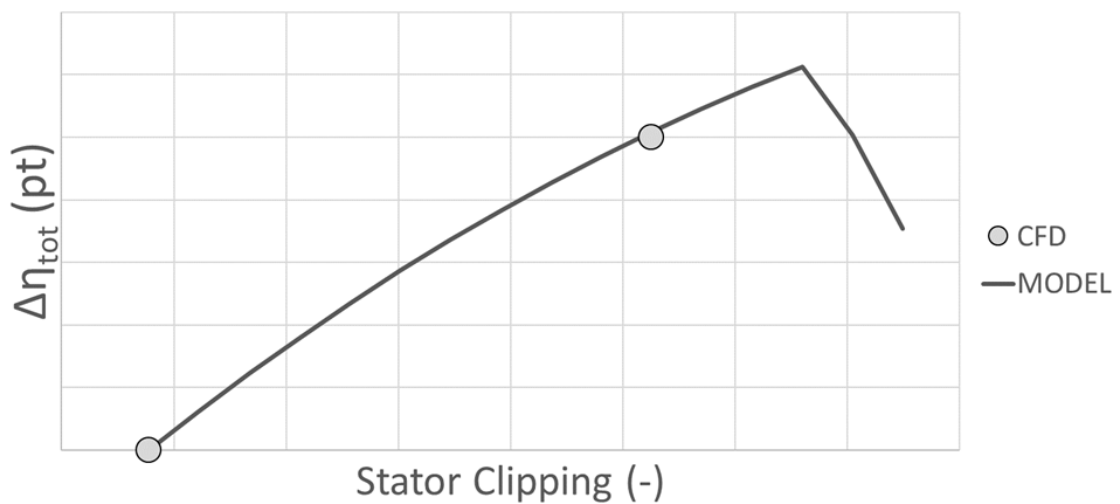
Figure 13 : Stator clipping effect on cruise efficiency predicted with the model, compared with CFD
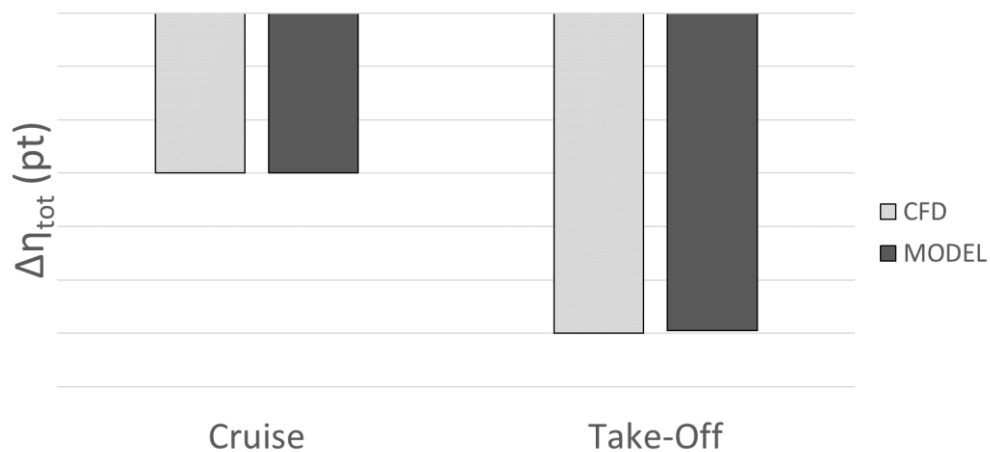
Figure 14 : Decreased number of blades (12/10 from 14/12) effect predicted by the model, compared with CFD

## 5. Conclusions

An analytical approach has been proposed to simulate the detailed aero performance behavior of the rotor and stator modules of an open fan engine architecture. This approach can be implemented using a limited number of CFD computations and simple calibrations of analytical expressions, enabling the modeling of the global rotor and stator performance. This method is sufficiently flexible and lightweight so that it can be directly integrated into thermodynamic cycle performance models, with almost instantaneous execution time and numerical robustness up to extreme operating conditions such as static, idle and reverse operation. Additionally, the approach offers the capability to explore blade geometry variations around the initial calibration, with good accuracy and limited effort when compared to full CFD design studies.

## References

[1] Lambey, M., N. Tantot, A. Binder, and A. Lebrun. 2019. Open Rotor Engines for Short/Medium Range Aircraft. ISABE-2019-24386.

[2] Dubosc, M., N. Tantot, P. Beaumier, and G. Delattre. 2014. A Method for Predicting Contra Rotating Propellers Off-design Performance. ASME GT2014-25057.

[3] Tantot, N., T. Brichler, M. Dubosc, and S. Ghebali. 2015. Innovative Approaches to Propellers off-design Performance Modeling. ASME GT2015-42145.

[4] Giannakakis, P., P. Laskaridis, T. Nikolaidis, and A. Kalfas. 2015. Toward a Scalable Propeller Map. *Journal of Propulsion and Power*. Vol. 31, No. 4, 1073–1082.

[5] Giannakakis, P., I. Goulos, P. Laskaridis, P. Pilidis, and A. Kalfas. 2016. Novel propeller map scaling method. *Journal of Propulsion and Power*. Vol. 32, No. 6, 1325-1332.

[6] Clark, R. A., C. Perron, J. C. Tai, B. J. Airdo, and D. N. Mavris. 2023. Development of an Open Rotor Propulsion System Model and Power Management Strategy. AIAA 2023-0309. *AIAA SCITECH 2023 Forum*.

[7] SAE International. 2012. AIR4065A - Propeller-Propfan In-flight Thrust Determination.

[8] Wald, Q. 2006. The aerodynamics of propellers. *Progress in Aerospace Sciences*, Vol. 42, Issue 2, 85-128.

[9] Anderson, J. D. 2011. Fundamentals of aerodynamics, 5th edition. *McGraw-Hill*. 416-417.